

Feature Extraction from Vein Images using Spatial Information and Chain Codes

Anika Pflug¹, Daniel Hartung² and Christoph Busch^{1,2}

`anika.pflug@cased.de`
`daniel.hartung@hig.no`
`christoph.busch@hig.no`

¹ University of Applied Sciences Darmstadt - CASED, Haardtring 100,
64295 Darmstadt, Germany

<http://www.h-da.de>

² Norwegian Information Security Laboratory (NISlab)

Høgskolen i Gjøvik, Teknologivn. 22,

2815 Gjøvik, Norway

<http://www.hig.no>

Abstract. The pattern formed by subcutaneous blood vessels is unique attribute of each individual and can therefore be used as a biometric characteristic. Exploiting the specific near infrared light absorption properties of blood, the capture procedure for this biometric characteristic is convenient and allows contact-less sensors. However, image skeletons extracted from vein images are often unstable, because the raw vein images suffer from low contrast. We propose a new chain code based feature encoding method, using spatial and orientation properties of vein patterns, which is capable of dealing with noisy and unstable image skeletons. Chain code comparison and a selection of preprocessing methods have been evaluated in a series of different experiments in single and multi-reference scenarios on two different vein image databases. The experiments showed that chain code comparison outperforms minutiae-based approaches and similarity based mix matching.

Keywords: biometrics, vein recognition, vascular recognition, chain code

1 Introduction

Intended to be a robust approach for liveness detection in fingerprint and hand geometry systems, vein recognition evolved to an independent biometric modality over the last decade. Classically the capturing process can be categorized in near and far infrared approaches. Vein recognition systems based on the near infrared approach are exploiting differences in the light absorption properties of the de-oxygenated blood flowing in subcutaneous blood vessels and the surrounding tissue. Veins become visible, as seen in figure 1, as dark tubular structures. They absorb higher quantities of the infrared light emitted by the LED of the sensor, than the surrounding tissue. Alternatively in the far infrared approach the heat

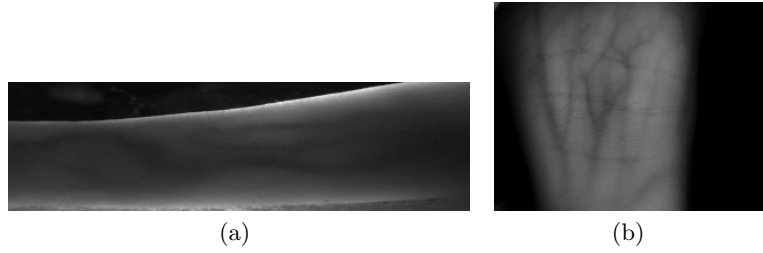


Fig. 1. Finger / wrist vein samples images from: (a) GUC45; (b) UC3M database.

radiation of the body can be measured. Because the temperature of blood is typically higher than the temperature of the surrounding tissue, the temperature gradient between the blood vessels and the tissue can be measured in this spectrum. Additionally, vein scanners can work contact-less, hence they are considered to be more hygienic than systems requiring direct physical contact. This makes them particularly suitable for applications in public areas.

Vein patterns evolve during the embryonic vasculogenesis. Their final structure is mainly influenced by the process of cell division and can therefore be expected to be random [7]. Even though scientific research about the uniqueness of vein patterns is sparse, many resources state that vein patterns are unique among individuals. Due to the fact, that the network of blood vessels forming the vein patterns is located underneath the skin, a vein pattern is hard to forge without the data subject's knowledge. Known approaches for forging vein patterns not only include the subject's knowledge but also his cooperation, such as shown in [38].

It is also expected, that the position of veins is constant over a whole lifetime [14]. Offering the same user convenience as fingerprints while being highly secure against forging, vein recognition has been applied in various fields of authentication and access control during the last years such as ATMs or airports. As a reaction to increasing misuse of bank cards for instance, a number of large banks in Japan integrated vein recognition systems into their ATMs [32]. The German logistics service DHL decided to use vein recognition for access control to high security areas at their new hub at Leipzig airport [33].

Still vein recognition faces challenges: limitations in capturing in-vivo images from the inside of the body, as well as ambient sunlight, temperature and varying skin properties like the pigmentation, or the thickness influence the image quality. As a result of all these factors the raw images delivered by the sensor have a low contrast, contain noise and a non-uniform brightness. Sophisticated algorithms for the preprocessing like contrast enhancement and segmentation as well as the final feature extraction and comparison are necessary to handle the variations and the noise.

In this paper we contribute a new chain code based feature extraction method and investigate its performance in combination with fusion techniques of image skeletons. The fusion aims at enhancing the biometric performance and

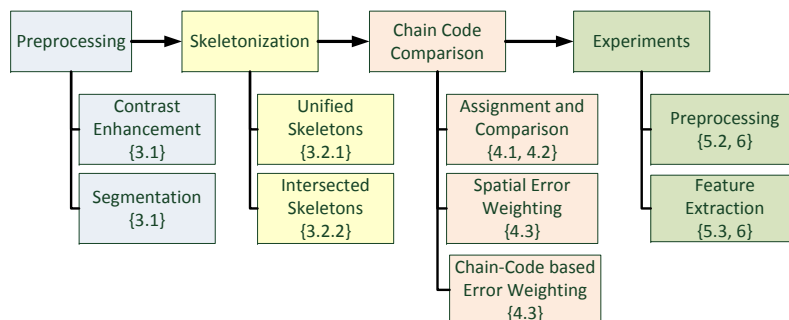


Fig. 2. Structure of this paper

the robustness against noise. Our approach is compared with minutiae-based feature extraction and a state-of-the-art geometry-based direct comparison approach. Moreover we measure the impact of different segmentation methods, image skeleton extractors and error weighting schemes on the biometric performance of our chain code based feature extractor. The experiments using finger vein images and wrist vein images showed that chain code comparison combined with skeleton fusing performs better than alternative direct comparison methods from the literature. An illustration of the work flow of our benchmark system in connection to the structure of this work is illustrated in Figure 2

The rest of this work is structured as follows. Section 2 will give an elaborate overview over relevant work in the field of vein recognition including work on the enhancement of vascular images. In Section 3, image enhancement, segmentation algorithms, the extraction of image skeletons and the skeleton fusing techniques used during the benchmarks in this paper will be described. After having introduced all necessary preprocessing steps, Section 4 will focus on the extraction and comparison of chain codes. The experiments and benchmarks conducted on the vein data will then be presented in Section 5. Finally Section 6 will conclude the paper with some future perspectives concerning vein recognition.

The paper extends the work from [13]. It contains an elaborate survey on the state of the art in the field of vein recognition and also introduces a new weighting scheme as an extension of the already published paper. Moreover we provide more details on the proposed algorithm and also present additional experimental results including the impact of skeleton pruning and the impact of different parameters on chain code comparison.

2 State-of-the-Art

Since the first suggestion to use the blood vessel network as a biometric characteristic was made more than one decade ago [17], a large number of different techniques for extracting and comparing vein patterns have been made. This

section gives an overview of preprocessing, feature extraction and comparison algorithms.

2.1 Preprocessing

As stated above, vein images tend to suffer from low contrast and noise. This raises the necessity for contrast enhancement methods. These methods suppress noise and enhance the local contrast of a vein image. Olsen achieved good results by using the STRESS algorithm [16, 21], which not only enhances the image's contrast but also balances irregular shading. A very fast and simple method for contrast enhancement is Wang and Leedham's normalization method [31]. It stretches the contrast by normalizing the grey values contained in the images but is not able to compensate irregular shading.

Another common problem with vein images is noise, which is hard to remove without losing information about the vein contours. Due to the imaging technique used by the sensor, the vein's edges are blurry. Deepika and Kandaswamy [6] solve this problem by using the non-linear diffusion method, which smoothens homogeneous image regions and preserves the vein's edges. The GSZ-Shock Filter used by Deepalmar and Madheswaran [5] can also be used for this purpose. If no explicit edge enhancement is needed, noise can be reduced by using a Gaussian filter [4] or dyadic wavelet transform [35].

Since many feature extraction algorithms work on image skeletons, the vein images must be segmented after the noise has been removed. A well-established histogram based segmentation approach was proposed by Otsu [22]. His method calculates a number of thresholds based on the grey level histogram in such a way that large quantities of similar grey values are considered as representing an object. Wang and Leedham [31] propose an algorithm called Adaptive Local Thresholds, which segments normalized images by using the local brightness information of the image. However this method has problems with blurry edges and low local contrast.

With their algorithms Repeated Line Tracking [19] and its successor Maximum Curvature Points [20], Miura and Nagasaka proposed two segmentation methods, which are robust to irregular shading and blurry edges. The maximum curvature points algorithm analyses brightness changes in cross-sectional image profiles and hence is not affected by a vein's width and brightness. Repeated Line Tracking starts at various random points in the vein image and follows light-coloured structures in the image. All pixels visited by the algorithm are tracked in a separate locus image, which is representing the location of the veins after the algorithms has terminated. A modified version of repeated line tracking is used by Yang et. al. [37].

A widely used segmentation algorithm in different applications for segmentation algorithms is the active contours method as proposed by Chan and Vese [3]. It has been applied to vein images of palm dorsa by Soni et. al. [25]. Active contours works with the principle of the intensity gradient. At least one initial shape is placed at a random point in the image before active contours moves,

splits, merges and warps this shape until it represents the contours of the veins displayed in the image.

A completely different approach to segmentation are filter based methods. Olsen achieved good segmentation results by using the standard technique of Laplacian of Gaussian [21], whereas Vlachos and Dermatas designed a dedicated compound filter, which is specialized in detecting horizontal, tubular structures [29]. A similar approach has been proposed in an earlier publication by Frangi et. al. [9], who also designed a special filter for detecting blood vessels in retina images.

2.2 Feature Extraction and Comparison

A multitude of different feature extractors and comparison algorithms have been proposed over time. This chapter categorizes different comparison algorithms applied in vein recognition following the features they are using. We differentiate between local comparison methods, which use certain details of the image for feature extraction, whereas holistic methods use whole images or image skeletons for comparison.

Holistic Methods One of the most famous holistic comparison methods is the principal component analysis (PCA), which is used in numerous pattern recognition tasks. In [15] Khan et. al. applied PCA on image skeletons derived from hand vein images. Principal component analysis can also be applied directly on enhanced images [30].

Xueyan et. al. derive vein descriptors using invariant moments for distinguishing the segmented vein images from different subjects. In [10] Guan et. al. have proposed to use bi-directional weighted modular PCA and compared the performance of different flavours of their algorithm with each other. In their studies, which were conducted with 132 subjects and a self-made capturing device, bi-directional weighted modular PCA showed the best performance among the other tested approaches. In a later approach Guan et. al. also evaluate the performance of an approach based on linear discriminant analysis on the same database, but could not improve the biometric performance with this approach [11].

All feature extraction and comparison algorithms enumerated so far are working with statistical properties of vein images. Chen et. al. [4] propose two algorithms for direct point-wise comparison, which overcome problems with affine transformations. Iterative Closest Point Matching (ICPM) is a modified version of the Iterative Closest Points algorithm for registering images. The second algorithm proposed by Chen et al., Similarity-based Mix-matching (SMM), compensates small translation and rotation errors by comparing the segmented version of one image with the image skeleton of the other one.

Yang and Li [36] propose a set of energy maps from the responses of steerable filters. Based on the amount of energy returned by a filter, they assign a grey value to each block of 5x5 pixels in the vein image. The resulting images with

each pixel representing the average response of a 5x5 block in the vein image are then compared bit pixel by pixel. They evaluate the performance of their feature extraction technique by using a database, which consists of 100 subjects, and showed that their approach performances other approaches. However they do not provide results using other databases.

In [18], Mirmohamadsadeghi and Drygajlo apply histograms of local binary patterns (LBP) as well as local derivative patterns (LDP) for feature extraction on palm vein images. In elaborate experiments they evaluated the behaviour of these descriptors under different constraints and also measured the performance of different distance measures for the histograms. They were able to achieve promising results with both descriptors, especially with a histogram intersection method.

Local Methods Known as established features from fingerprints, minutiae have also been used for extracting features from skeletonized vein images [28]. Because minutiae are composed of spatial coordinates, they are subject to translation and rotation. This issue is addressed by projecting minutiae points into frequency space [34], where translation gets eliminated and rotation becomes translation. Spectral minutiae have also been applied to vein recognition [28] in different variants. SML performs an element-wise comparison of two minutiae-spectra in frequency space, whereas SML fast Rotate (SMLFR) compares the spectra while trying different translations of them. However the number of minutiae contained in the image can be very small. Instead of comparing their positions directly, it is also possible to use the distances between all minutiae as features [30]. Wang further proposes to use the line segments, which are separated by endpoints and bifurcations [31]. Fan et. al. propose to use the watershed algorithm for detecting dominant points from a vein image [8]. Three different filters generate a multi resolution representations of these dominant points, which serve as features.

3 Preprocessing

3.1 Contrast Enhancement and Segmentation

As already mentioned, all vein images have to be enhanced in a preprocessing stage before features can be extracted from the image. The vein images used during our experiments are first enhanced by using adaptive non-local means taken from [26] followed by the noise suppressing and edge enhancing non-linear diffusion algorithm [1].

The image enhancement step is followed by a segmentation step. In order to see, if there is an image segmentation method, which is particularly suitable for segmenting vein images, three different segmentation methods have been compared. The first of these methods is Otsu's histogram-based segmentation [22]. Additionally the active contours algorithm proposed by Chan and Vese [3] and the multi-scale filter method by Frangi et. al. [9] have been tested on the finger vein images.

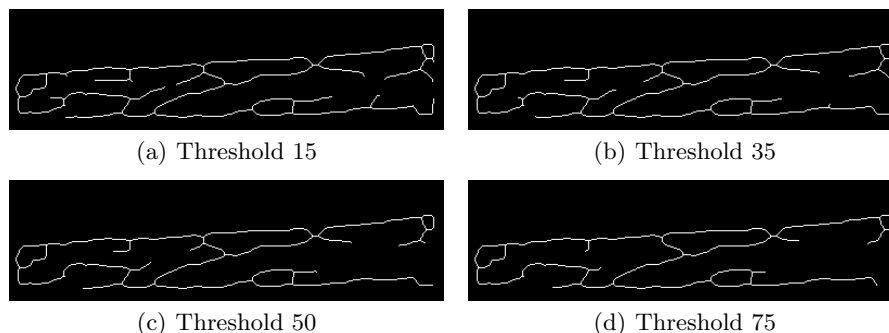


Fig. 3. Skeletons extracted by fast marching skeletonization methods using different thresholds. The higher the threshold the more details are cut off from the skeleton.

3.2 Skeletonization

In the approaches we used in our experiments, skeleton images are the basis for feature extraction. Because of noise and poor contrast, these skeletons can look different, even though they come from the same biometric source. In order to improve the reliability of the extracted image skeletons and hence the reliability of the extracted features, we propose to use fast marching skeletonization as proposed in [27] in combination two different approaches for fusing multiple skeletons to a single one. The goal is to create a more stable version than any of the input skeletons.

In fast marching skeletonization incremental indices are assigned to each pixel on the edge of the figure. Then they are collapsed until only the center line is left. From the difference between two neighbouring indices in the collapsed figure, a local weight of a branch can be determined. For those part of the image skeleton, derived from center part of the figure, the difference between the indices is high and so is their weight. These fine-grained branches are likely to be artifacts, which were introduced by segmentation errors or noise and can be removed by applying a threshold. All skeleton points where the difference between their indices falls below the threshold are deleted. All other points are kept. Hence, depending on the threshold, more or less of these remote branches are cut off. The larger the threshold value, the more details are removed (see Figure 3).

3.3 Skeleton Fusing

In order to further enhance the stability of skeletons, we propose two basic fusing techniques. The first one is called skeleton unification and produces a skeleton which possesses all branches and details, of the input skeletons. The second one, called skeleton intersecting, combines a variable number of input skeletons and delivers combined skeletons which possess only the branches which the majority of the input skeletons has in common. The goal is to create a more stable version than any of the input skeletons.

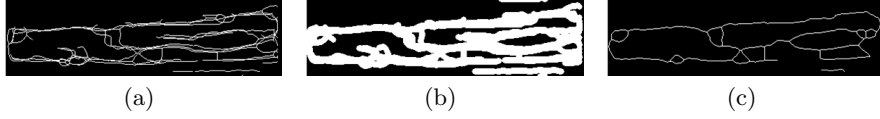


Fig. 4. Fusion based on unification (GUC45 samples) using $n = 3$ input skeletons: (a) superimposed structure S_{uni_1} ; (b) disk-shape structuring element dilated structure S_{uni_2} ; (c) final unified skeleton S_{uni} .

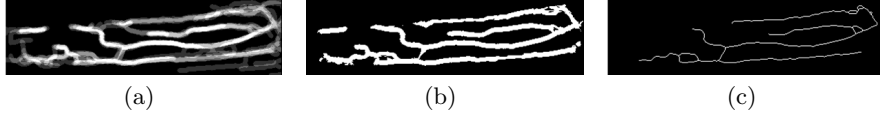


Fig. 5. Fusion based on intersection (GUC45 samples) with $n = 5$ input skeletons and threshold $t = 3$: (a) dilated density structure S_{int_2} ; (b) S_{int_3} (threshold t applied to segment S_{int_2}); (c) final intersection skeleton S_{int} .

Unified Skeletons For deriving a unified skeleton it takes n input skeletons, where n was set to 3 in our experiments. In a first step, all input skeletons $S_i(x, y)$ are aligned using ICP [24] and then super-imposed to a common structure S_{uni_1} (Fig. 4(a)).

$$S_{\text{uni}_1}(x, y) = \cup_{i=1}^n S_i(x, y) \quad (1)$$

The registered input skeletons are fused together by dilating the superimposed figure S_{uni_1} with a disk-shaped structuring element (Fig. 4(b)) to get S_{uni_2} . Afterwards the fast marching skeletonization algorithm [27] is applied to the dilated figure in order to create the unified skeleton S_{uni} (Fig. 4(c)).

Intersected Skeletons The second proposed algorithm creates an intersected skeleton, which possesses only those features which occur in at least t of the input skeletons. An example for skeleton intersection with $n = 5$ input skeletons is illustrated in Figure 5. The intersected skeleton in Figure 5 consists of the lines which occur in at least three of the five input skeletons ($t \geq 3$).

Similarly to the unification approach, the input skeletons S_i need to be aligned to each other. Then each of the n input skeletons is dilated with a disk-shaped structuring element, creating binary structures S_{int_1} . These dilated skeletons are then added up to form a common unified density structure called S_{int_2} .

$$S_{\text{int}_2}(x, y) = \sum_n S_{\text{int}_{1n}}(x, y) \quad (2)$$

S_{int_2} contains values between 0 and n . All input skeletons having a pixel that is classified as vein at position (x, y) in case of $S_{\text{int}_2} = n$ and 0, meaning that none of the input skeletons has any veins at this coordinate. Now a threshold value t with $1 \leq t \leq n$ is applied to S_{int_2} resulting in S_{int_3} . In this step all pixels

which at least occur t times in the input skeletons are kept, all other pixels are set to zero.

$$S_{\text{int}_3}(x, y) = \begin{cases} 1 & \text{for } S_{\text{int}_2} \geq t \\ 0 & \text{else} \end{cases} \quad (3)$$

Finally the fast marching skeletonization is applied again, which results in the intersected skeleton S_{int} .

4 Chain Code Comparison

Similarities between two image skeletons can be determined by measuring the relative positions of the skeleton lines as well as their relative orientation. Two lines, which are parallel should be considered to be more similar than two non-parallel skeleton lines. Chain code based feature extraction uses the position of each pixel on a skeleton line in combination with its local orientation reflected by the chain code value for feature encoding. This enables the algorithm to find associated points between the probe and the reference skeleton and to measure parallelism.

4.1 Preliminaries and Chain Code Assignment

Before chain code values can be assigned to an image skeleton, some preliminaries have to be met. In a first step the probe and the reference skeleton have to be aligned with each other. As for skeleton fusing, we used ICP for skeleton alignment. Moreover all points where veins split up (bifurcations) have to be removed from the image skeleton in order to avoid ambiguities. To make sure all chain codes refer to a common starting point, a reading direction has to be defined. In our work, chain code extraction started from the bottom left corner of the image and ended at the top right corner. If the reading direction is fixed, chain codes extracted from the same shape with different coordinates will be identical. After the skeletons are computed, the feature extraction module iterates over each pixel (x, y) of the skeleton starting from the bottom left corner. Each skeleton pixel is assigned a chain code value according to the relative position of its successor in reading direction (see Figure 6). The chain code assignment for each pixel indexed by its coordinates x and y in the skeleton image I_{skel} is defined as

$$C(x, y) = \begin{cases} 1 & \text{if } I_{\text{skel}}(x + 1, y) = 1 \\ 3 & \text{if } I_{\text{skel}}(x + 1, y + 1) = 1 \\ 5 & \text{if } I_{\text{skel}}(x, y + 1) = 1 \\ 7 & \text{if } I_{\text{skel}}(x - 1, y + 1) = 1 \\ 9 & \text{if } I_{\text{skel}}(x - 1, y) = 1 \\ 0 & \text{else} \end{cases} \quad (4)$$

4.2 Comparison

After chain code assignment, the similarity between two aligned chain codes C and C' is calculated. The algorithm tries to find pairs of associated points by searching in orthogonal direction to the local orientation of the chain code value stored at the currently examined point. The search for associated pixels stops if either an associated point could be found or if the maximum search depth d_{max} is exceeded. When a pair of associated skeleton points has been found, their similarity is calculated based on their spatial distance d and the chain code difference c . Where (x, y) and (x', y') are the coordinates of the two associated points and $C(x, y)$ and $C'(x', y')$ are their chain code values.

$$d = \sqrt{|x - x'|^2 + |y - y'|^2} \quad (5)$$

$$c = |C(x, y) - C'(x', y')|^2 \quad (6)$$

The local error E at the point (x, y) is then calculated as follows.

$$E(x, y) = \frac{d + c}{E_{max}} \quad (7)$$

$$E_{max} = \frac{d_{max} + c_{max}}{2} \quad (8)$$

The values for d_{max} and c_{max} denote the maximum search depth and the maximum possible difference between two chain code values. Following Equation 6 and the scheme sketched in Figure 6, $c_{max} = 8^2 = 64$. The local error is stored at position (x, y) in an error map E , which has the same size as the input images.

The assignment of associated points is depending on the order of the two skeletons to be compared (probe/reference). If we start with the reference skeleton and search for an associated pixel in the probe skeleton, a different pixel pair can be identified as if we would have started the other way around. This also means that the local error depends on the order of the two skeletons. This is handled by computing two error maps E_1 and E_2 . E_1 contains all local errors calculated by using C as reference and C' as probe skeleton and E_2 contains all local errors using C' as probe and C as reference, respectively. The total error map E_{total} is the sum of local errors for each point in the skeleton images and is computed as follows:

$$E_{total}(x, y) = E_1(x, y) + E_2(x, y) \quad (9)$$

Finally the similarity score of the skeletons to compare is defined as:

$$Score = 1 - \frac{\sum_x \sum_y E_{total}(x, y)}{\sum_x \sum_y E_{max}} \quad (10)$$

An example of how a point pair can be found by using the local chain code value is shown in Figure 6(b). The algorithm starts at the boldly bordered point

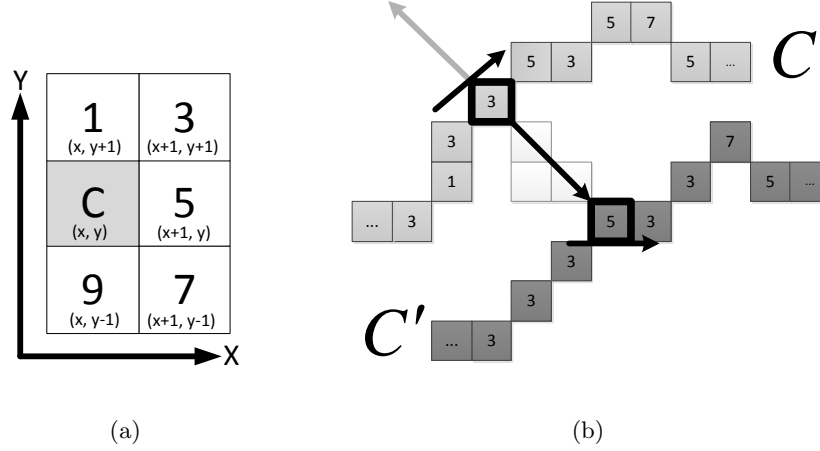


Fig. 6. Chain code extraction scheme for feature extraction from prepared image skeletons and calculation of local error using the spacial distance between two associated pixels and the chain code difference

in C and searches in orthogonal direction for a corresponding point in C' . After two mated points have been identified, their local error, which is a value between 0 (no error) and 2 (maximum error) is calculated. The global distance measure between all points in C and C' is, as stated before, the weighted sum of all local errors.

4.3 Error Weights

Caused by the position of the infrared-LEDs in the sensor and the human physiology, the contrast is not the same throughout the image region. Especially the edge regions of the image are typically darker than the center region of the image, which means that local error extracted from the center regions of the image are more likely to be reliable than local error in the edge regions. In order to take this into account a weighting function $\omega_1(x, y)$ is introduced which assigns higher weights to the local errors in the center regions of the image. It calculates a weight for each local error according to its position in the image. *width* represents the total width of the image. An threshold value t is defined, which specifies the image region where the weight of the local error decreases. We assigned an error weight smaller than one to the leftmost quarter of errors and the rightmost quarter of error respectively. Hence the value 0.25 for t was used here. w denotes the total with of the image.

$$\omega_1(x, y) = \begin{cases} \frac{y-x}{w-t} & \text{if } x < w - t \\ \frac{t-x}{t} & \text{if } x > t \\ 1 & \text{else} \end{cases} \quad (11)$$

Another possibility of error weighting is based on the fact that most veins in our finger vein image are horizontal, which is caused by the architecture of the sensor. Hence, the portability of being a noise artifacts is assumed to be higher, the more a chain code value differs from horizontal orientation. As the local chain codes for the veins have already been assigned, this information can additionally be used for applying a weighting factor based on the local orientation of a line, namely the local chain code value. As mentioned above, chain code values already indicate the local orientation of a skeleton line, hence the local error can also be weighted using the chain code values. ω_2 calculates a weighting factor for each error depending on the chain code value C in the comparison image. The constant h represents the chain code value assigned to a line with horizontal orientation. For our chain code extraction scheme, h is set to 5.

$$\omega_2(C) = \begin{cases} 1 - (C - h)^2 & \text{if } C \neq h \\ 1 & \text{else} \end{cases} \quad (12)$$

5 Experimental Setup

All experiments were conducted on the basis of a modular vein verification system implemented in MATLAB. The benchmark system allows for arbitrary combinations of different segmentation, feature extraction and comparison modules. The main quality measure used for benchmarking different pipeline configurations is the equal error rate (EER). We conducted two different experiments, one covering aspects of preprocessing in connection with chain code comparison and the second one dealing with the comparison of selected feature extraction, error weighting and comparison approaches. Information about both experiments and the databases which were used during the evaluation is provided in this section.

5.1 Vein Databases

In the experiments two different vein databases were used. Their main properties are summarized in Table 1. In both cases the images were captured with a CCD-camera and illuminated with NIR light at a wavelength of 850nm. The GUC45 dataset contains finger vein images from 45 data subjects collected at Gjøvik University College in Norway over a long period of time. Each finger, including the thumbs, was captured two times during each of the 12 sessions, which results in 10800 unique vein images in total. The images from GUC45 suffer from low contrast and high noise, which makes it hard for any algorithm to extract stable skeletons and hence to achieve a low error rate on this data. However this fact makes them particularly interesting for research purposes as it allows for exploring the limitations of algorithms for feature extraction and comparison.

The second database, called UC3M, consists of wrist vein images, which were collected as described in [23]. The focus of this experiment was to evaluate the effect of different illumination intensities on the visibility of veins. For each of the

29 users, 6 images were taken for each hand under three different illumination settings. This results into 348 images in total.

Database	GUC45	UC3M*
Frequency Band	NIR (850nm)	
Sensor	non-commercial	
Modality	Finger (10)	Wrist (2)
Data Subjects	45	29
Sessions	12	1
Images per Session	10×2	2×6
Images	10800	348
Resolution (px)	$512 \times 240^\dagger$	640×480
Depth	8 Bit gray-scale	

Table 1. Properties of the biometric vein datasets used in the experimental section. [†]For the experiment the images are cropped to size 468×122 to eliminate most non-finger area. *Details published in [23].

5.2 Preprocessing

The preprocessing stage consists of three steps, namely image enhancement, segmentation and skeletonization. During image enhancement, noise should be removed and at the same time image contrast should be enhanced. In order to meet both criteria, different methods are combined. In a first step, the vein images are enhanced with adaptive non-local means as proposed by Struc and Pavesic [26] followed by non-linear diffusion for noise suppressing and edge enhancement [1].

The image enhancement step is followed by a segmentation step. In order to see, if there is an image segmentation method, which is particularly suitable for segmenting vein images, three different segmentation methods have been benchmarked. The first of these methods is Otsu’s histogram-based segmentation [22]. Additionally the active contours algorithm proposed by Chan and Vese [3] and the multi-scale filter method by Frangi et. al. [9] have been tested on the vein images.

Preprocessing is concluded by the skeletonization approach proposed by Telea and van Wijk [27]. For determining the influence of skeleton pruning on the EER, we compared the biometric performance of different pipelines using chain code comparison and Otsu’s segmentation algorithm with different thresholds during the skeletonization step.

5.3 Feature Extraction Evaluation

For comparing the biometric performance of chain code comparison to other feature extraction methods, we evaluated chain code comparison on GUC45 and UC3M. We compared the performance to the evaluation results of spectral minutiae (SML and SMLFR) as proposed in [12], Similarity-based Mix-Matching (SMM) [4] and the performance of chain code comparison on single references and fused skeletons. In all experiments using fused skeletons, the fused skeleton served as the reference image and a skeleton extracted from one vein image was used as the probe image.

We investigate the influence of the maximum search distance on the error rate of chain code comparison and evaluated the discriminating potential of spatial and chain code distance. Furthermore evaluate the influence of the previously introduced error weighting schemes on the EER. For doing this we configured a pipeline using Otsu’s segmentation algorithm, fast marching skeletonization with a threshold of 35 and chain code comparison for feature extraction.

6 Results

In our experiments, the segmentation algorithms came to slightly different results, but had a minor effect on the overall system’s performance. The measured performance difference between the different segmentation algorithms on GUC45 is less than 2% points in terms of the EER. The main difference between the evaluated segmentation approaches was in terms of computation time, however the approach by Frangi and Niessen performed slightly better on the UC3M dataset.

In contrast to the preprocessing step, the impact of the feature extraction and comparison method is significant. Table 2 summarizes the performance measures for each of the datasets. The results for GUC45 were obtained using Otsu’s segmentation algorithm, whereas the EER measures on UC3M are based on Frangi and Niessen’s filter-based approach. For each of the evaluated configurations we measured the EER and the operating point for 0.1% FAR. Furthermore we provide the 90% confidence intervals for each of the measured performance indicators.

The images in GUC45 have a particularly low contrast and therefore cannot be expected to give good biometric performance. However, GUC45 is a challenge for all tested algorithms. In addition, it also contains multiple samples per subject. The results of the different feature extraction and comparison approaches on GUC45 are summarized in Figure 7. The best performance could be achieved with chain code comparison using unified skeletons as reference samples and skeletons derived from only one image as probes. This configuration was named Fused Union. With an EER of 24.67% Fused Union outperformed all other configurations including SMM, but also single reference chain code comparison. This shows that already a simple skeleton fusing approach like the proposed one, enhances the quality of image skeletons and improves the system performance.

None of the error weighting schemes has an effect on the performance of chain code comparison. On average, ω_2 had a slightly better performance than ω_1 , but the confidence value indicate that there is no statistically significant difference between these two configurations.

Further investigations on the performance of Fused Union for each finger on GUC45 showed, that the fingers of the left hand appear to be more suited for vein recognition than the right hand fingers (see Figure 7(b)). In our experiments, the highest error rate was measured with images from the thumbs (Fingers indices 5 and 6). The EER of configurations using intersected skeletons increases the more input skeletons are used. A reason for this could be that unstable skeletons have only few intersecting parts, which results in fused skeletons with low details. Less details however mean less discriminative power and results in increasing error rates.

For the UC3M dataset an excellent biometric performance could be measured without the skeleton fusion techniques proposed. SMM and the chain code algorithm perform at the same level (EER around 1% EER). Skeleton fusion could reduce the EER to 0.63%, whereas skeleton intersection with $n = 3$ and $t = 2$ yielded an EER of 0.67%.

Whereas the segmentation did not have any effect on the EER, the level of detail in the skeletons had a measurable effect on the performance of chain code comparison. Figure 7(c) shows, that a careful selection of the threshold during fast marching skeletonization can deliver a considerable improvement of the overall performance. The lowest EER could be achieved when using a threshold of 35. The performance obtained from other thresholds is similar and moves around approximately 31% EER. The only outlier is the threshold 5. The reason for this are artifacts, introduces by fast marching skeletonization during the assignment of indices. These artifacts are removed when applying thresholds above 15, but are still part of the skeleton for low thresholds.

Experiments on the behaviour of chain code comparison using different search depths showed, that the careful choice of this parameter is crucial, as the spatial distance between two skeleton points appeared to have a larger impact on the biometric performance than the difference between two adjacent chain codes. The reason for this is that there the possible variance between two chain code values is small compared to the variance of the spatial distance. The maximum search depth should be chosen according to the resolution of the input vein images and the expected density of the vein patterns. For GUC and UC3M a maximum search depth of 9 pixels delivered the best performance.

7 Conclusion and Future Work

The proposed chain code algorithm as well as the state of the art SMM [4] algorithm perform very similar on the chosen datasets, it seems the quality of the images is a limiting factor here. Only a multi-reference approach could further improve the results.

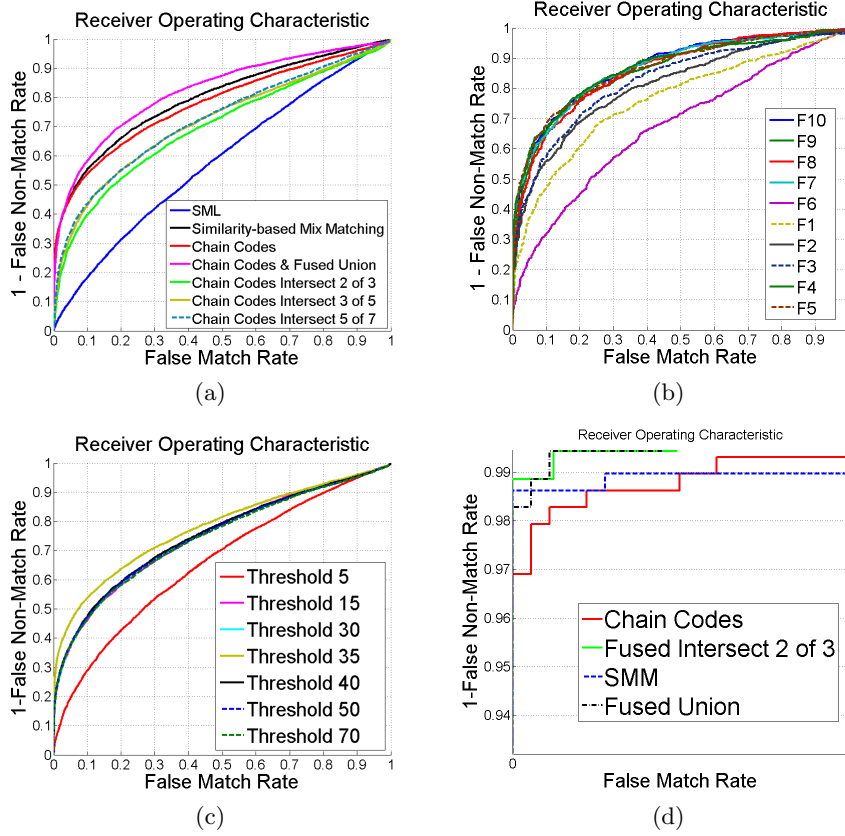


Fig. 7. ROC curves for (a) selection of feature extraction algorithms and (b) *Fused Union* configuration, different finger samples from GUC45 dataset. Finger indices are assigned according to the ISO-standard [2] with indices 1 until 5 for the right hand fingers in indices 6 until 10 for the left hand fingers, where counting always starts from the thumbs. (c) shows ROC curves for a selection of different thresholds in fast marching skeletonization using chain code comparison. (d) shows ROC curves for chain code pipelines and SMM on the UC3M dataset

Comparison Algorithm	GUC45		UC3M	
	EER	OP	EER	OP
Chain Codes	29.06 (± 0.73)	77.97 (± 0.67)	1.38 (± 1.27)	3.10 (± 1.68)
Chain Codes with ω_1	29.42 (± 0.89)	78.65 (± 0.66)	1.38 (± 1.13)	1.72 (± 1.26)
Chain Codes with ω_2	28.44 (± 0.72)	77.041 (± 0.68)	2.07 (± 1.37)	4.48 (± 1.99)
Fused Union	25.21 (± 0.71)	84.15 (± 0.62)	0.63 (± 0.87)	1.72 (± 1.62)
Fused Intersect t=2, n=3	34.49 (± 0.89)	95.60 (± 0.34)	0.67 (± 1.10)	1.15 (± 1.33)
Fused Intersect t=3, n=5	32.87 (± 0.92)	93.71 (± 0.43)	NA	NA
Fused Intersect t=5, n=7	32.20 (± 0.97)	97.27 (± 0.31)	NA	NA
SMM	27.84 (± 0.71)	78.40 (± 1.13)	1.38 (± 0.67)	1.38 (± 1.13)
SML	39.089	NA	6.13	NA
SMLFR	40.25	NA	5.90	NA

Table 2. Benchmark results (EER in % and OP) for finger vein (GUC45) and wrist images (UC3M). The numbers in brackets after each result are the 90% confidence interval for the results. NA: not measured in the experiments.

Even though the proposed comparison on Fused Union skeletons showed promising results, the algorithm’s time wise performance is not impressive compared to other feature extraction and comparison algorithms. Future work focuses on reducing the required computing time by replacing the pixel-based chain code extraction with a convolution-based approach and by selecting less reference points for skeleton registration and comparison in order to further decrease the size of the feature vector.

Further improvements could also be made by extending the error calculation to complete line segments in order to make chain code comparison less sensitive to single outliers and more sensitive to mismatching line segments. Moreover, additional simulations on different vein datasets will also show the feasibility of the approach for different vein modalities.

References

1. *Applications of Nonlinear Diffusion in Image Processing and Computer Vision* (2001), vol. Vol. LXX, Acta Math. Univ. Comenianae.
2. ISO/IEC 19795-1:2006 Information Technology *Biometric Data Interchange Formats - Part 2: Finger Minutiae Data*, March 2005.
3. CHAN, T. F., AND VESE, L. Active Contours Without Edges. *IEEE Transactions on Image processing* 10, 2 (February 2001), 266–277.
4. CHEN, H., LU, G., AND WANG, R. A New Palm Vein Method Based on ICP Algorithm. In *International Conference on Informaion Systems* (November 2009).
5. DEEPPALMAR, M., AND MADHESWARAN, M. An Improved Multimodal Palm Vein Recognition System Using Shape and Texture Features. *International Journal of Computer Theory and Engineering* 2, 3 (June 2010), 1793–8201.
6. DEEPIKA, C. L., AND KANDASWAMY, A. An Algorithm for Improved Accuracy in unimodal Biometric Systems Through Fusion of Multiple Feature Sets. *ICGST-GVIP Journal* 9, 3 (June 2009), 33–40.

7. EICHMANN, A., YUAN, L., MOYON, D., LENOBLE, F., PARDANAUD, L., AND BRANT, C. Vascular Development: From Precursor Cells to Branched Arterial and Venous Networks. *International Journal of Developmental Biology* 49 (2005), 259–267.
8. FAN, K.-C., LIN, C.-L., AND LEE, W.-L. Biometric Verification Using thermal Images of Palm-Dorsa Vein-patterns. In *16th IPPR Conference on Computer Vision, Graphics and Image Processing* (2003).
9. FRANGI, R. F., NIESSEN, W. J., VINCKEN, K. L., AND VIERGEVER, M. A. Multi-scale Vessel Enhancement Filtering. In *Medical Image Computing and Computer-Assisted Intervention*. Springer-Verlag, 1998, pp. 130–137.
10. GUAN, F., WANG, K., AND WU, Q. Bi-directional weighted modular b2dpca for finger vein recognition. In *Image and Signal Processing (CISP), 2010 3rd International Congress on* (oct. 2010), vol. 1, pp. 93–97.
11. GUAN, F., WANG, K., AND YANG, Q. A study of two direction weighted (2d)2lda for finger vein recognition. In *Image and Signal Processing (CISP), 2011 4th International Congress on* (oct. 2011), vol. 2, pp. 860–864.
12. HARTUNG, D., OLSEN, M. A., XU, H., AND BUSCH, C. Spectral Minutiae for Vein Pattern Recognition. In *The IEEE International Joint Conference on Biometrics (IJCB)* (2011).
13. HARTUNG, D., PFLUG, A., AND BUSCH, C. Feature extraction from vein images using spatial information and chain codes. In *GI Sicherheit 2012* (March 2012), Lecture Notes in Computer Science, Gesellschaft fr Informatik (GI).
14. JOUSSEN, A. M. Vascular plasticity—the role of the angiopoietins in modulating ocular angiogenesis. *Graefes Arch Clin Exp Ophthalmology* 239, 12 (December 2001 Dec), 972–975.
15. KHAN, M. H.-M., AND KHAN, N. M. Feature Extraction of Dorsal hand- Vein Pattern Using a Fast Modified PCA Algorithm Based on Cholesky Decomposition and Lanczos Technique. *International Journal of Mathematical and Computer Sciences* 5, 4 (2009), 230–234.
16. KOLÅS, Ø., FARUP, I., AND RIZZI, A. Stress: A New Spatial Colour Algorithm (submitted 2011).
17. KONO, M., H, H. U., AND UMEMURA, S. A new method for the identification of individuals by using vein pattern matching of a finger. In *Proceedings of the 5th symposium on pattern measurement* (Yamaguchi, Japan, 2000), pp. 9–12.
18. MIRMOHAMADSADEGHI, L., AND DRYGAJLO, A. Palm vein recognition with local binary patterns and local derivative patterns. In *Biometrics (IJCB), 2011 International Joint Conference on* (oct. 2011), pp. 1–6.
19. MIURA, N., NAGASAKA, A., AND MIYATAKE, T. Feature Extraction of Finger-vein Patterns Based on Repeated Line Tracking and its Application to Personal Identification. *Machine Vision and Applications* 15 (Juli 2004), 194–203.
20. MIURA, N., NAGASAKA, A., AND MIYATAKE, T. Extraction of Finger-Vein Patterns Using Maximum Curvature Points in Image Profiles. *IEICE - Transactions on Information and Systems E90-D*, 8 (August 2007), 1185–1194.
21. OLSEN, M., HARTUNG, D., BUSCH, C., AND LARSEN, R. Contrast Enhancement and Metrics for Biometric Vein Pattern Recognition. In *ICIC* (2010).
22. OTSU, N. A Threshold Selection Method from Grey-Level Histograms. *Systems, Man and Cybernetics, IEEE Transactions* 9 (January 1979), 62–66.
23. PASCUAL, S., J.E., URIARTE-ANTONIO, J., SANCHEZ-REILLO, R., AND LORENZ, M. Capturing Hand or Wrist Vein Images for Biometric Authentication Using Low-Cost Devices. In *Intelligent Information Hiding and Multimedia Signal Processing (IIH-MSP), 2010 Sixth International Conference on* (october 2010), pp. 318–322.

24. RUSINKIEWICZ, S., AND LEVOY, M. Efficient Variants of the ICP Algorithm. Tech. rep., Stanford University, 2001.
25. SONI, M., GUPTA, S., AND RAO, M. A New Vein Pattern-based Verification System. *International Journal of Computer Science and Information Security* 8, 1 (2010), 58–63.
26. STRUC, V., AND PAVESIC, N. Illumination Invariant Face Recognition by Non-local Smoothing. In *Proceedings of the BIODID Multicomm* (September 2008).
27. TELEA, A., AND VAN WIJK, J. J. An Augmented Fast Marching Method for Computing Skeletons and Centerlines. In *Joint Eurographics - IEEE TCVG Symposium on visualization* (2002).
28. URIARTE-ANTONIO, J., HARTUNG, D., PASCUAL, J., AND SANCHEZ-REILLO, R. Vascular biometrics based on a minutiae extraction approach. In *Security Technology (ICCST), 2011 IEEE International Carnahan Conference on* (oct. 2011), pp. 1–7.
29. VLACHOS, M., AND DERMATAS, E. Vein Segmentation in Infrared Images Using Compound Enhancing and Crisp Clustering. *Lecture Notes in Computer Science 5008/2008* (2008), 393–402.
30. WANG, K., ZHANG, Y., YUAN, Z., AND ZHUANG, D. Hand Vein Recognition Based on Multi Supplemental Features of Multi-Classifer Fusion Detection. In *International Conference on Mechatronics and Automation* (June 2006).
31. WANG, L., AND LEEDHAM, G. A Thermal Hand Vein Pattern Verification System. *LNCS: Pattern Recognition and Image Analysis 3687/2005* (2005), 58–65.
32. WATANABE, M., AND ENDOH, T. Palm Vein Authentication Technology and its Applications. In *Proceedings of the Biometric Consortium Conference* (September 2005).
33. WITOPIL, K. Schutzmanahmen im Leipziger DHL-Hub. *Protector 6* (June 2008), 44–45.
34. XU, H., AND VELDHUIS, R. N. Spectral Minutae: A Fixed-length Representation of a Minutae Set. In *IEEE Computer Society Conference on Computer Vision and Pattern Recognition Workshops* (2008), pp. 1–6.
35. XUEYAN, L., SHUXU, G., AND FENGLI, G. Vein Pattern Recognition by Moment Invariants. In *1st Conference on Bioinformatics and Biomedical Engineering* (July 2007).
36. YANG, J., AND LI, X. Efficient finger vein localization and recognition. In *Pattern Recognition (ICPR), 2010 20th International Conference on* (aug. 2010), pp. 1148–1151.
37. YANG, W., XU, X., AND LIAO, Q. Personal Authentication Using Finger Vein Patterns and Finger-Dorsa Texture Fusion. In *MM '09 Proceedings of the 17th ACM international conference on Multimedia* (2009).
38. ZENO GERADTS, P. S., Ed. *FIDIS - Future of Identity in the Information Society* (2006).